JOURNAL OF MATERIALS SCIENCE 30 (1995) 4584–4590

Preparation and properties of *X*-sialon

Y. ZHOU, J. VLEUGELS, T. LAOUI, P. RATCHEV, O. VAN DER BIEST
Department of Metallurgy and Materials Engineering, Katholieke Universiteit Leuven, De Croylaan 2, B-3001 Leuven, Belgium

X-sialon has been produced by hot pressing Si_3N_4–Al_2O_3–SiO_2 powder mixtures and Si_3N_4 powder–mullite gel mixtures at 1650 °C. The formation mechanism of *X*-sialon has been studied and is correlated with the processing technique for the two preparation routes. Microprobe analysis of the obtained *X*-sialon phase, combined with previous observed compositions and literature formulae suggests that, at 1650 °C, *X*-sialon exists as a narrow solid solubility region on the Si_3N_4–mullite line in the Si_3N_4–SiO_2–Al_2O_3–AlN phase diagram. The physical, mechanical and chemical properties of *X*-sialon have been evaluated. *X*-sialon has a modest hardness of 1280 kg mm^{-2}, a fracture toughness of 1.7 MPa m$^{1/2}$, and an elastic modulus of 213 GPa. *X*-sialon exhibits excellent chemical stability in contact with iron-based alloys at 1200 °C.

1. Introduction

Although the Si_3N_4–Al_2O_3–AlN–SiO_2 system has been the subject of extensive research during the last 30 years, only very few papers concerning *X*-sialon have been published.

The exact chemical composition of *X*-sialon and its position in the quaternary phase diagram has been controversial for a long time. Compositions, obtained by different analysis techniques on samples prepared from different starting powders by different fabrication routes, range between 42 and 60 eq % aluminium and 42 and 84 eq % oxygen. The compositions found in the literature [1–12] are given in Table I and are plotted on the phase diagram in Fig. 1. The composition reported by Naik *et al.* [1], $Si_{12}Al_{18}O_{39}N_8$, was suggested to be a closer formula, rather than $Si_3Al_6O_{12}N_2$ or $Si_2Al_3O_7N$ [13].

Most of the work done concerns *X*-ray diffraction (XRD) and transmission electron microscopy (TEM) studies, trying to determine the complex crystal structure of *X*-sialon. Monoclinic [7], triclinic [2, 14] and orthorhombic [15] unit cells are reported. According to Thompson and Korgul [14], a difference has to be made between a high-*X* form, rapidly crystallizing at lower temperatures from a supercooled highly viscous silica rich sialon liquid, and a low-*X* form, prepared by slow cooling from the melt.

Pure *X*-sialon is hard to obtain because of the uncertainty about the exact chemical composition, the difficulty of avoiding weight loss during densification and the fact that different fabrication routes can result in different products. Most of the work has been done on *X*-sialon samples obtained from reaction sintered powder mixtures in the Si_3N_4–Al_2O_3–AlN–SiO_2 system. Recently, a new fabrication route, through simultaneous carbothermal reduction and nitridation of kaolinite at 1500 °C, was described [13].

Very little is known about the chemical and mechanical properties of pure *X*-sialon. The density was reported to be 3.00 g cm^{-3} [3]. The linear thermal expansion coefficient was found to be in the range of $3.7 \times 10^{-6} - 4.5 \times 10^{-6}$ °C^{-1} [16]. *X*-sialon is stable at temperatures up to 1730 °C under N_2 atmosphere [4], and the melting point was estimated to be about 1720 °C [1].

It was suggested that the presence of *X*-sialon in an *X*–β′-sialon composite is detrimental to the mechanical properties, since it reduces the strength as well as the toughness of the sialon material [5].

The aim of the present paper is the preparation and analysis of the chemical composition and mechanical properties of *X*-sialon: the hardness, fracture toughness and elastic modulus of *X*-sialon are measured and the chemical compatibility with steels is studied by interaction couples at high temperature. A suggestion about a possible formation mechanism of *X*-sialon is given.

2. Experimental procedure

In this work, *X*-sialon is prepared by conventional hot pressing of Si_3N_4–Al_2O_3–SiO_2 powder mixtures and Si_3N_4 powder–mullite gel mixtures.

The overall chemical composition of the starting mixtures was $Si_{12}Al_{18}O_{39}N_8$, the closest literature formula to the electron microprobe analysis on *X*-sialon containing ceramics [6].

Commercial Si_3N_4 powder, HCStarck grade LC 12-SX (97 % α, submicrometre particle size, 1.8–2.1 wt % oxygen), Al_2O_3 powder, Baikowski grade SM8 (95 % α, submicrometre particle size) and Sigma fumed SiO_2 (submicrometre size) were used to prepare the powder mixtures. A 100 g of powder was mixed on a multi-directional mixer for 72 h in a polyethylene bottle containing 350 g alumina milling balls and 1 l *n*-propanol.

0022–2461

TABLE I Chemical compositions of *X*-sialon found in literature

Composition	Al (eq %)	O (eq %)	Reference
Solubility region	52–56	65–67	[7]
$SiAlO_2N$	43	57	[8]
$Si_6Al_6O_9N_8$	43	43	[9]
$Si_3Al_6O_{12}N_2$	60	79	[5]
$Si_7Al_9O_{23}N_3$	49	84	[10]
$Si_4Al_4O_{11}N_2$	43	78	[11]
$Si_{10}Al_{15}O_{32}N_7$	53	75	[2]
$Si_{12}Al_{18}O_{39}N_8$	53	77	[1]
$Si_2Al_3O_7N_1$	53	82	[3]
$Si_6Al_{10}O_{21}N_4$	56	78	[12]
$Si_{12.0}Al_{17.9}O_{40.9}N_{6.7}$	53	80	[4]
$Si_{12.0}Al_{21.1}O_{45.8}N_{6.8}$	57	82	[4]
$Si_{12}Al_{18}O_{36}N_{10}$	53	71	[4]
$Si_{16.4}Al_{23.6}O_{48.8}N_{11.2}$	52	74	[6]
$Si_{16.8}Al_{22.4}O_{47.8}N_{13.0}$	50	71	[6]
$Si_{16.9}Al_{22.7}O_{48.8}N_{11.6}$	50	74	[6]

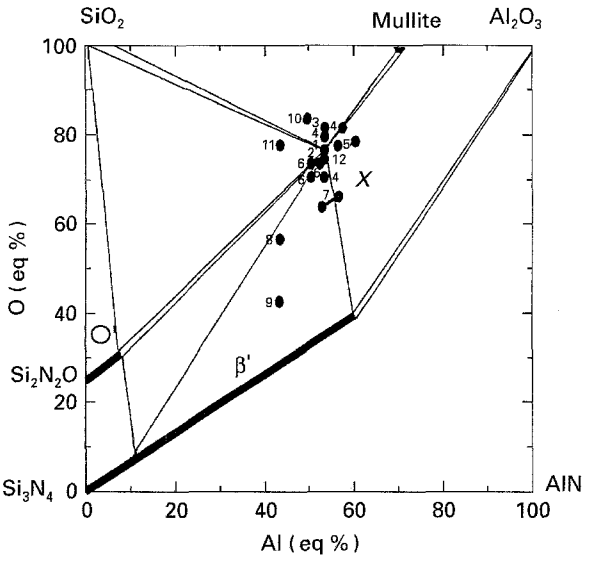

Figure 1 Chemical compositions of *X*-sialon found in literature, plotted on the Si_3N_4–Al_2O_3–AlN–SiO_2 subsolidus phase diagram [1]. The numbers on the diagram refer to the literature references, the corresponding chemical formulae can be found in Table I.

In another preparation method, Si_3N_4 powder was dispersed into a sol–gel mullite solution. The mullite precursor was prepared by mixing tetraethyl orthosilicate [$Si(OC_2H_5)_4$] and aluminium nitrate nonahydrate [$Al(NO_3)_3.9H_2O$] which was already dissolved in ethanol [17]. The Si_3N_4 powder was added to the solution. To obtain a homogeneous dispersion of the Si_3N_4 powder, different mixing methods were used, as will be explained later.

After evaporation of the propanol in the powder mixture method and burning-out the organic species in the sol–gel method, 12 g of the dry mixture was inserted into a graphite container, coated with boron nitride. After cold pressing at 40 MPa, the samples were hot pressed in vacuum (0.1 Pa) for 1 h at 1650 °C, under a uniaxial load of 30 MPa. Although no special care was taken of the nitrogen pressure in the hot press, the weight loss of the samples was less than 2%.

Phase identification was done by *X*-ray diffraction, using Diffrac 11 programs on XRD patterns acquired on a Philips diffractometer equipped with a CuK_α source. Although the JCPDS diffraction files 34–719, 35–23, 31–32 and 36–832 could all be used to identify *X*-sialon, diffraction file 35–23 was preferred because of the more complete indexed reference pattern.

Scanning electron microscopy (SEM, Jeol 733 microprobe) and TEM (Jeol 200 CX) were used for microstructural characterization. Quantitative chemical analysis was done by electron microprobe analysis (EPMA), using a pure SiO_2 and Al_2O_3 standard. Samples and standards were coated simultaneously with a very thin gold layer, to ensure a homogeneous coating thickness and X-ray absorption interaction. Quantitative analysis was performed for silicon, aluminium (EDS, Tracor Northern) and oxygen (WDS, Jeol 733). Nitrogen was calculated by difference. Samples for TEM were prepared by mechanical thinning, dimpling and then ion milling with an argon beam. Ion milled foils were coated with carbon for examination in the TEM operating at 200 kV.

The density of the specimens was determined by the water displacement method.

The elastic modulus of the specimens was measured by the resonance frequency method [18], using a Grindo-sonic apparatus.

Vickers hardness was measured on a Zwick hardness tester. The reported values are the mean of five indentations.

Fracture toughness, K_{IC}, values were obtained by the Vickers indentation technique, based on crack length measurements of the radial crack pattern produced by Vickers hardness indentations. Toughness values were calculated using the formula of Anstis *et al.* [19]

$$K_{IC} = 0.016\,(E/H)^{1/2}\,P/c^{3/2}$$

with E, the elastic modulus; H, the hardness; P, the indentation load; and c, the radial crack length.

The chemical compatibility between *X*-sialon or *X*-sialon containing ceramics and iron-based alloys is assessed by pressing together under a small load (2.5 MPa) polished slices of ceramic and steel at elevated temperatures and assessing the extent of interdiffusion of species between the two materials. The interaction couples were heated in vacuum ($\approx$0.1 Pa) at 1200 °C. The holding time was variable and cooling was performed as quickly as possible.

3. Results and discussion

3.1. *X*-sialon obtained from Si_3N_4–Al_2O_3–SiO_2 powder mixtures

From optical microscopy observations, the samples reached full density, i.e. no porosity was observed. The measured density of the samples, only containing *X*-sialon diffraction peaks according to XRD analysis, was 3.04 g cm^{-3}.

The microstructure of the obtained samples was investigated by SEM on both polished and fractured surfaces. The presence of a small amount of silicon rich particles (less than 5 wt %) with a lower oxygen content than the *X*-sialon matrix, that could not be

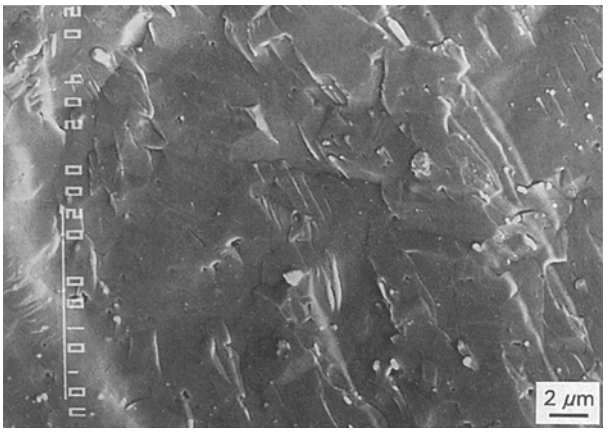

Figure 2 Presence of Si_3N_4 particles on a fractured *X*-sialon surface obtained from the powder mixture method.

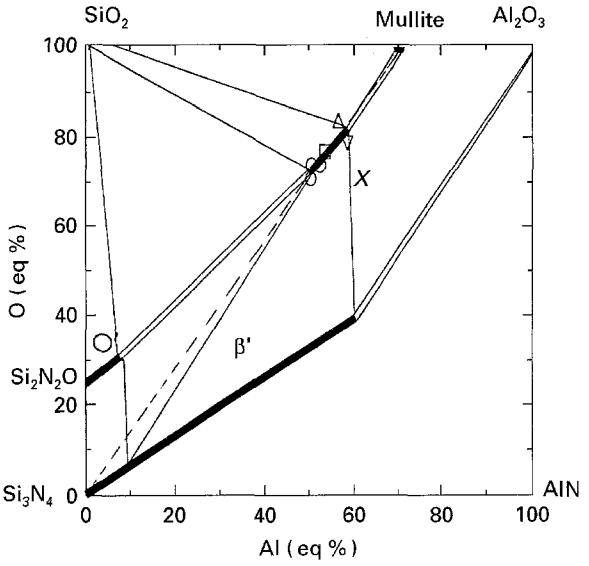

Figure 3 *X*-sialon solid solubility region at 1650 °C: (○) chemical compositions found in the multiphase sialon ceramics [6]; (△) composition obtained from the powder mixture method and (▽) from the Si_3N_4 (powder)–mullite (sol–gel) method; (□) $Si_{12}Al_{18}O_{39}N_8$, the composition reported by Naik *et al.* [1]. The dashed line shows the link of Si_3N_4 and mullite.

etched away by fluoric acid, were found and are considered to be Si_3N_4 particles. Fig. 2 shows these particles on a fractured *X*-sialon surface.

From electron microprobe analysis, the overall chemical composition of *X*-sialon was found to be $Si_{14.13}Al_{24.45}O_{54.43}N_{7.00}$, which is more towards the mullite side on the phase diagram (see Figs 1 and 3), compared to the compositions measured in the multiphase sialon ceramics [6] and the formula of Naik *et al.* [1].

The Vickers hardness and fracture toughness values for *X*-sialon are given in Table II. The measured elastic modulus is 213 GPa, which is very close to that of Si_2N_2O, being 222 GPa [20]. Assuming a similar strength and thermal conductivity, the combination of the lower Young's modulus and lower thermal expansion coefficient [16] might indicate that *X*-sialon can have a better thermal shock resistance than alumina.

TABLE II Vickers hardness HV and fracture toughness, K_{IC}, of *X*-sialon obtained from an Si_3N_4–Al_2O_3–SiO_2 powder mixture (PM) and an Si_3N_4 (powder) – mullite (sol–gel) mixture (PGM)

Indentation load (kg)	HV (kg mm^{-2})		K_{IC} (MPa m$^{1/2}$)	
	PM	PGM	PM	PGM
1	1290	1329	1.25	1.17
3	1268	1267	1.29	1.13
5	1280	1252	1.44	1.16
10	1267	–	1.76	–

TABLE III Mixing conditions and relative amounts of formed phases, as estimated from XRD analysis, in the hot pressed samples obtained from Si_3N_4 (powder) – mullite (sol–gel) mixtures.

Mixing condition	*X*-sialon (%)	Mullite (%)	Si_3N_4 (%)
Magnetic stirring (poor mixing)	48	40	12
Ball milling for 72 h (relatively good mixing)	63	24	13
Ball milling for 72 h, followed by ultrasonification and magnetical stirring (good mixing)	85	15	Negligible

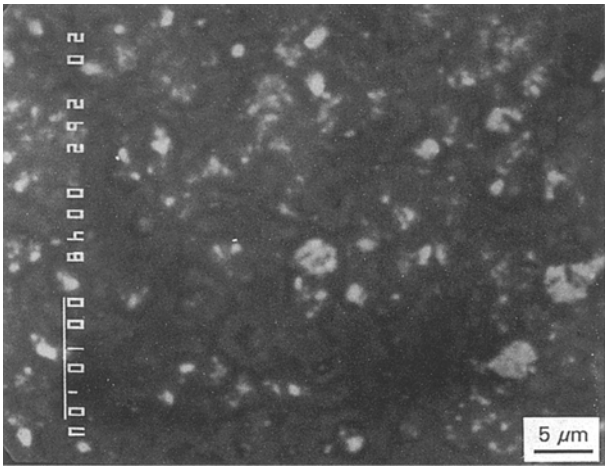

Figure 4 *X*-sialon (dark) formed in between Si_3N_4 (white) agglomerates and mullite (grey matrix) from the Si_3N_4 (powder)–mullite (sol–gel) method.

3.2. *X*-sialon obtained from Si_3N_4 (powder)–mullite (sol–gel) mixtures

In the Si_3N_4 (powder)–mullite (sol–gel) method, the microstructure, phase content and homogeneity of the hot pressed samples is strongly influenced by the mixing conditions, as summarized in Table III.

Magnetic stirring of the Si_3N_4 powder, dispersed in the mullite precursors, resulted in an inhomogeneous microstructure containing large agglomerates of unreacted Si_3N_4 and mullite. *X*-sialon was formed in between the Si_3N_4 and the mullite, as shown in Fig. 4.

Ball milling for 48 h of the dispersed Si_3N_4 powder improved homogeneity in the hot pressed samples. Mullite agglomerates were reduced, whereas the *X*-sialon content increased.

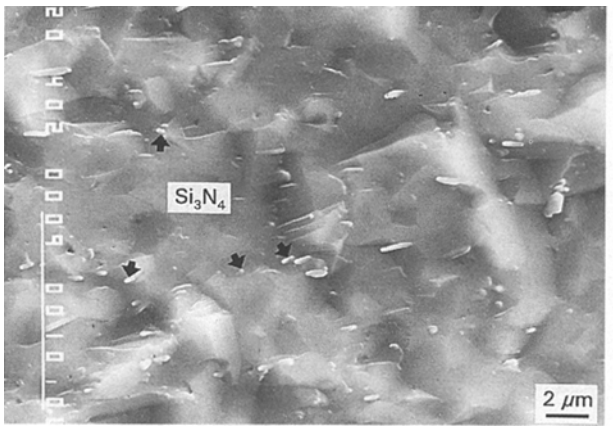

Figure 5 A fractured surface of *X*-sialon obtained from the Si_3N_4 (powder)–mullite (sol–gel) method. Arrows indicate small Si_3N_4 particles.

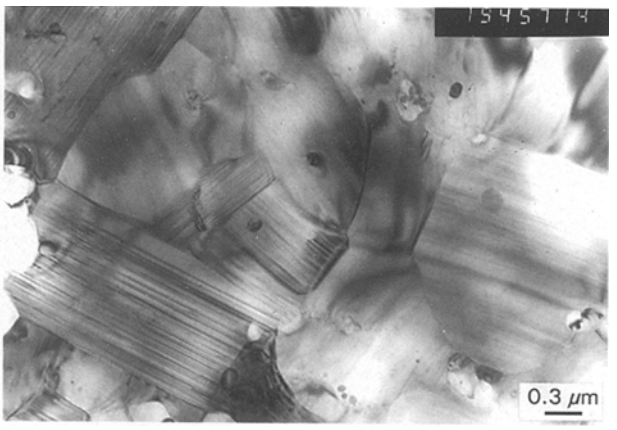

Figure 6 Transmission electron micrograph of the hot pressed Si_3N_4–Al_2O_3–SiO_2 powder mixture.

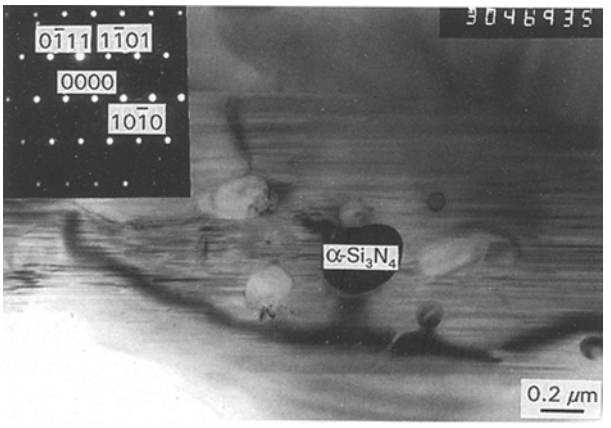

Figure 7 Transmission electron micrograph showing a particle identified by SAD as α-Si_3N_4 in orientation $1\,\bar{2}\,1\,\bar{3}$.

The best mixing procedure was obtained when the ball milled mixture was ultrasonificated just before magnetically stirring during gellation. No apparent agglomerates could be found in the dense samples and the amount of unreacted Si_3N_4 was negligible. The obtained ceramic contained 10–15% mullite, as estimated from XRD analysis.

The effect of mixing on *X*-sialon formation from Si_3N_4 (powder)–mullite (sol–gel) mixtures is modelled for two extreme mixing conditions in Section 3.5.

SEM observation revealed also the presence of Si_3N_4 particles on both polished and fractured surfaces, as shown in Fig. 5.

The mechanical properties of the ceramic obtained by the powder–sol–gel method are listed in Table II. Hardness and fracture toughness are comparable to those obtained for *X*-sialon prepared by the powder mixture method.

The chemical composition of *X*-sialon, $Si_{13.86}Al_{25.18}O_{51.85}N_{9.11}$, is similar to the composition obtained in the powder mixture method (see Fig. 3). Both compositions are close to $Si_{12.0}Al_{21.2}O_{45.8}N_{6.8}$, one of the formulae proposed by Bergmann *et al.* [4].

Based on EPMA results of the *X*-sialon ceramics in this study, the chemical composition of the *X*-sialon grains in multiphase ceramics [6] and the formulae reported in the literature, it might be concluded that at 1650 °C, *X*-sialon exists as a narrow solid solubility region on the Si_3N_4-mullite line in the Si_3N_4–Al_2O_3–AlN–SiO_2 phase diagram, as shown in Fig. 3.

3.3. Transmission electron microscopy observations

The microstructural characterization of the ceramics prepared by both processing routes mentioned above was done by TEM.

Fig. 6 shows the microstructure of the hot pressed Si_3N_4–Al_2O_3–SiO_2 powder mixture. Within the resolution limits of the microscope, no intergranular amorphous phase could be observed at the grain boundaries or in the triple junctions of the microstructure.

The *X*-sialon grains, easily identified by their twin patterns, have an average grain size of 3 μm. In addition to the *X*-grains, small particles of size approximately 0.1 μm were observed, mainly within the *X* grains and occasionally at the grain boundaries. Selected area diffraction (SAD) analysis performed on these small grains revealed that they were mainly α-Si_3N_4 particles, remaining from the starting powder. Fig. 7 shows such a particle, identified by means of SAD as α-Si_3N_4 within a *X*-sialon grain in orientation $1\,\bar{2}\,1\,\bar{3}$. In addition to the identified α-Si_3N_4 particles, small amounts of β-Si_3N_4 could not be ruled out, as it was not possible to unequivocally identify all investigated particles, since the unit cell parameters in the *a* direction of the hexagonal structure of α-Si_3N_4 and β-Si_3N_4 are rather close (0.775–0.777 nm for α-Si_3N_4 and 0.759–0.761 nm for β-Si_3N_4) [21]. On the other hand, in order to exclude completely the presence of β-Si_3N_4 much bigger statistics are needed. Occasionally, one can find *X*-sialon grains free of Si_3N_4 inclusions.

The microstructure of the *X*-sialon ceramic obtained from uniformly dispersed Si_3N_4 powder in sol–gel mullite, mainly consists of *X*-sialon with mullite as a minor phase, as shown in Fig. 8. The average grain size of the *X* grains is similar to that in the sample prepared by the powder mixture method. Si_3N_4 particles (mainly α-Si_3N_4) were also observed within the *X*-sialon grains, as shown in Fig. 9.

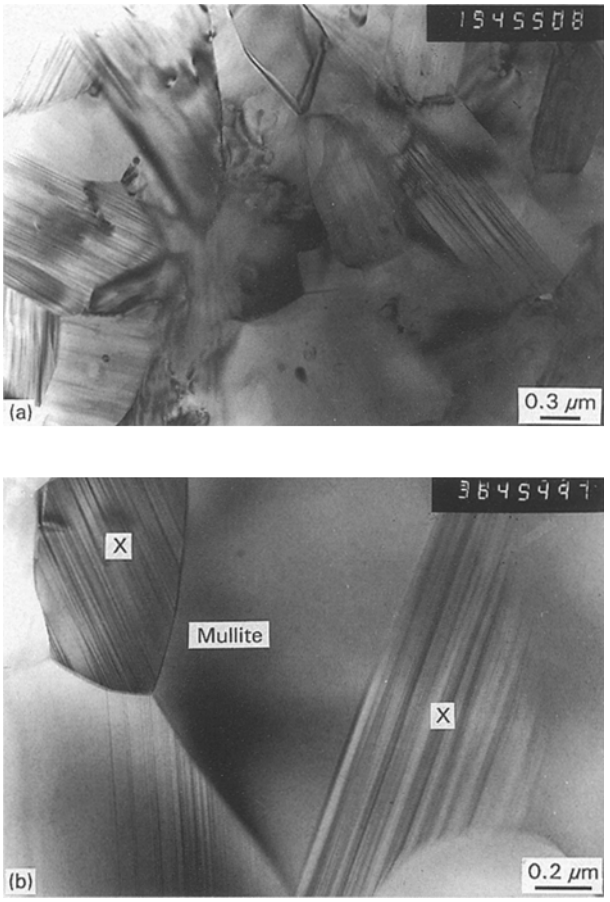

Figure 8 Transmission electron micrograph of the hot pressed Si_3N_4 (powder)–mullite (sol–gel) mixture, showing *X*-sialon grains (major phase) and mullite grains (minor phase) at low magnification (a) and high magnification (b).

Figure 9 Transmission electron micrograph of the hot pressed Si_3N_4 (powder)–mullite (sol–gel) mixture, showing the presence of unreacted Si_3N_4 particles.

3.4. A possible formation mechanism of *X*-sialon

Based on the microstructural observations, the following formation mechanism for *X*-sialon can be proposed.

In the Si_3N_4–Al_2O_3–SiO_2 powder mixture method, the Al_2O_3 and SiO_2 additives will form a viscous oxynitride glass with the SiO_2 layer around the α-Si_3N_4 particles. At higher temperatures, the α-Si_3N_4 particles dissolve into this melt, which will crystallize as *X*-sialon during cooling below 1650 °C.

In the Si_3N_4 (powder)–mullite (sol–gel) mixture method, the formation mechanism of *X*-sialon is thought to consist of the following steps. The first step is the crystallization of the mullite gel. This can already start at 1000 °C [17]. The presence of mullite as an intermediate phase could be confirmed by XRD analysis of samples heated at 1500 °C. Once formed, mullite should be stable up to 1800 °C according to the SiO_2–Al_2O_3 phase diagram. However, as the temperature increases, mullite forms a viscous phase with the SiO_2 impurity on the surface of the Si_3N_4 powder. Mullite and Si_3N_4 progressively dissolve into this silicon aluminium oxynitride phase, that will crystallize as *X*-sialon during cooling from the melt below 1650 °C.

The reason for the presence of Si_3N_4 particles (mainly α-Si_3N_4) scattered throughout the sample and within the *X*-sialon grains suggests that the dissolution of Si_3N_4 was not complete in both processing routes. It could be assumed that the nucleation and growth of *X*-sialon initiates from these undissolved α-Si_3N_4 particles during cooling. A similar situation was found for Si_2N_2O materials obtained from Si_3N_4–SiO_2 mixtures with different sinter additives, where small inclusions, identified as α-Si_3N_4, were thought to act as nucleation sites for Si_2N_2O [22].

3.5. Effect of mixing on *X*-sialon formation from Si_3N_4 (powder)–mullite (sol–gel) mixtures

In the Si_3N_4 (powder)–mullite (sol–gel) method, the obtained microstructure is strongly influenced by the mixing conditions as already explained in Section 3.2.

Fig. 10 shows a schematic model representing the formation process of *X*-sialon at two extreme mixing conditions. The mullite gel consists of a structure similar to a glass material, i.e. a three-dimensional random network with short-range arrangements of SiO_2 and Al_2O_3 polyhedra. The mullite gel can start crystallizing at 1000 °C [17].

When the Si_3N_4 powder is dispersed as agglomerates into the mullite gel (see Fig. 10a), Si_3N_4 agglomerates will still be present in a mullite matrix after mullite crystallization. As the temperature is further increased, mullite and silicon nitrides will progressively dissolve in the amorphous aluminium silicon oxynitride phase that will be formed. However, the Si_3N_4 agglomerates cannot be dissolved completely, resulting in the crystallization of *X*-sialon in between the Si_3N_4 agglomerates and the surrounding mullite matrix during cooling. The obtained microstructure is shown in Fig. 4.

However, if the Si_3N_4 powder can be dispersed as individual particles in the mullite precursors (see Fig. 10b), The dissolution of mullite and Si_3N_4 in the oxynitride glass will be complete and a single phase *X*-sialon ceramic will be formed after cooling from the melt.

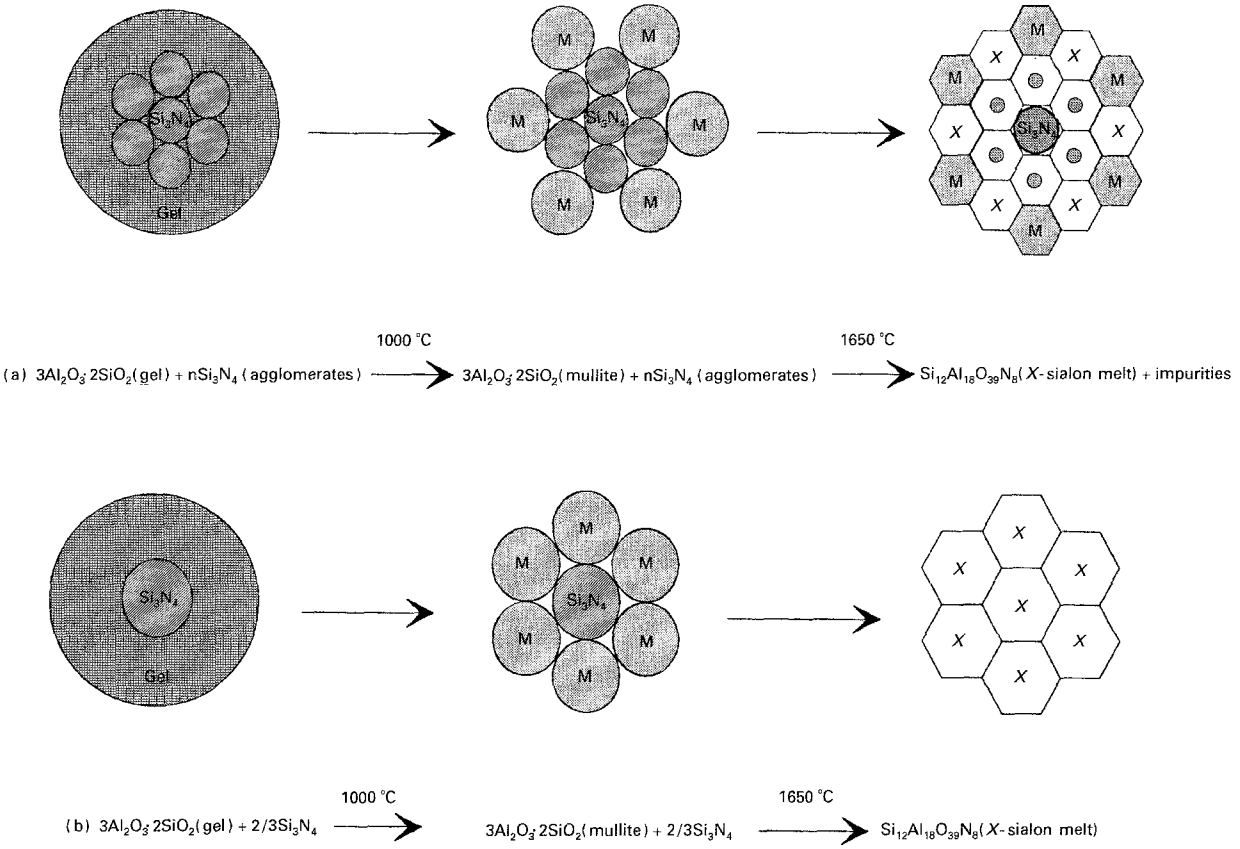

Figure 10 Schematic models of *X* phase formation from the Si_3N_4 (powder)–mullite (M) (sol–gel) mixture, showing the effect of mixing degree on formation of *X* phase: (a) under poor mixing, formation of *X* phase is inhibited by mullite agglomerates performed at lower temperature; and (b) under good mixing, pure *X* phase sialon is obtained by a complete reaction between intermediate phase of mullite and starting Si_3N_4 powder.

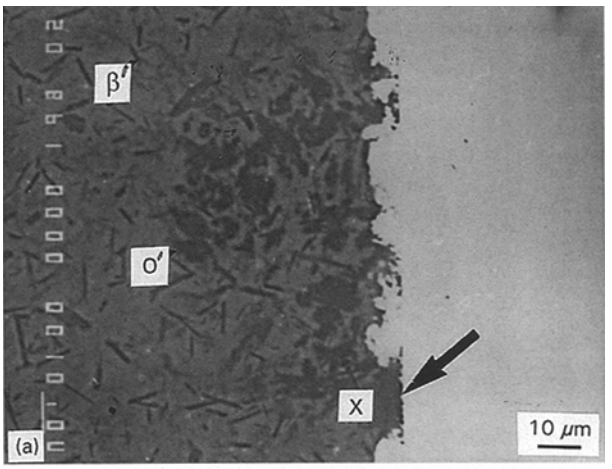

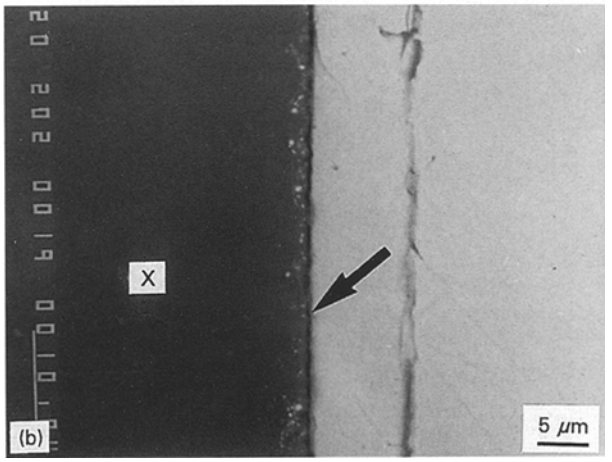

3.6. Chemical compatibility with steel

Unreacted *X*-sialon grains were found in the interaction layers between multiphase β′–O′–*X*-sialon ceramics with several iron-based alloys. In some regions, agglomerates of *X*-sialon grains were able to prevent the interaction, as shown in Fig. 11a for the interaction between a β′–O′–*X*-sialon ceramic and pure iron after 3 h at 1200 °C. The cross-sectioned interaction couple between *X*-sialon obtained by the powder mixture method and DIN 42CrMo4 steel after 5 h at 1200 °C showed no or very limited reactivity, as can be seen in Fig. 11b.

The limited chemical interaction with iron-based alloys might be explained by the high free energy of formation of *X*-sialon. This free energy was estimated to be $-23\,808.261 + 5.454\,T\ kJ\,mol^{-1}$ $Si_{12}Al_{18}O_{39}N_8$ [23].

4. Conclusions

X-sialon ceramics can be produced by hot pressing Si_3N_4–Al_2O_3–SiO_2 powder mixtures or Si_3N_4 (powder)–mullite (sol–gel) mixtures.

α-Si_3N_4 inclusions were found in the *X*-sialon grains of the ceramics obtained from both processing

Figure 11 (a) *X*-sialon grains preventing the interaction between a β′–O′–X-sialon ceramic and pure iron, and (b) the cross-sectioned interaction couple between pure *X*-sialon and DIN 42CrMo4 steel after 5 h at 1200 °C. Arrows indicate the position of the initial contact plane.

routes. These Si_3N_4 inclusions originate from undissolved starting powder and are thought to act as nucleation sites for *X*-sialon.

The microstructure of the ceramics obtained by the Si_3N_4 (powder)–mullite (sol–gel) method, is strongly influenced by the mixing conditions. The crystallization of mullite from the mullite gel is an intermediate step in this processing method.

From the EPMA results of this study, combined with previous reported chemical compositions of *X*-sialon, it is clear that, at 1650 °C, *X*-sialon exists as a narrow solid solubility region on the line between silicon nitride and mullite in the Si_3N_4–Al_2O_3–AlN–SiO_2 phase diagram.

X-sialon exhibits a modest hardness of 1280 kg mm^{-2} and toughness of 1.2 MPa $m^{1/2}$. The elastic modulus was measured to be 213 GPa. *X*-sialon was found to be chemically stable in contact with iron-based alloys at 1200 °C.

Acknowledgements

This work was supported by the Brite-Euram programme of the Commission of the European Communities under project BREU-0096-C. J. V. thanks the Belgian IWONL fund for a research fellowship.

References

1. I. K. NAIK, L. J. GAUCKLER and T. Y. TIEN, *J. Amer. Ceram. Soc.* **61** (1978) 332.
2. A. ZANGVIL, *J. Mater. Sci. Lett.* **13** (1978) 1370.
3. A. ZANGVIL, L. J. GAUCKLER and M. RUHLE, *ibid.* **15** (1980) 788.
4. B. BERGMAN, T. EKSTRÖM and A. MICSKI, *J. Eur. Ceram. Soc.* **8** (1991) 141.
5. R. R. WILLS, R. W. STEWART and J. M. WIMMER, *Amer. Ceram. Soc. Bull.* **56** (1977) 194.
6. J. VLEUGELS and O. VAN DER BIEST, *J. Eur. Ceram. Soc.* **13** (1994) 529.
7. K. H. JACK, *J. Mater. Sci.* **11** (1976) 1135.
8. *Idem, Trans. J. Brit. Ceram. Soc.* **72** (1973) 376.
9. Y. OYAMA, *Yogyo-Kyokai-Shi* **82** (1974) 351.
10. M. MITOMO, Y. HASEGAWA, Y. BANDO, A. WATANABE and H. SUZUKI, *ibid.* **88** (1980) 298.
11. L. J. GAUCKLER, H. L. LUKAS and G. PETZOW, *J. Amer. Ceram. Soc.* **58** (1975) 346.
12. Powder Diffraction file card No. 36–832. Joint Committee for Powder Diffraction Standards-International Centre for Diffraction Data, 1601 Park Lane, Swarthmore.
13. C. C. ANYA and A. HENDRY, *J. Eur. Ceram. Soc.* **10** (1992) 65.
14. D. P. THOMPSON and P. KORGUL, in "Progress in Nitrogen Ceramics", edited by F. L. Riley (Martinus Nijhoff, The Hague, Netherlands, 1983) p. 375.
15. E. GUGEL, I. PETZENHAUSER and A. FICKEL, *Powder Met. Int.* **7** (1075) 66.
16. I. IWAO and O. TOSHITAKA, *Adv. Ceram. Mater.* **2** (1987) 784.
17. K. OKADA and N. OTSUKA, *J. Amer. Ceram. Soc.* **69** (1986) 652.
18. NBN B 15–230, "Niet-destructieve proeven, meting van de resonantiefrekwentie", Belgisch Instituut voor Normalisatie, juni (1976).
19. G. R. ANSTIS, P. CHANTIKUL, B. R. LAWN and D. B. MARSHALL, *J. Amer. Ceram. Soc.* **64** (1981) 533.
20. P. BOCH and J. C. GLANDUS, *J. Mater. Sci.* **14** (1979) 379.
21. G. ZIEGLER, J. HEINRICH and G. WÖTTING, *ibid.* **22** (1987) 3041.
22. W. BRAUE, R. PLEGER and W. LUXEM, in "Silicon Nitride 93, Proceedings of the International Conference on Silicon Nitride-Based Ceramics," Stuttgart, October, edited by M. J. Hoffmann, P. F. Becher and G. Petzow (Trans Tech Publications, Aedermannsdorf, Switzerland, 1993).
23. P. DÖRNER, L. GAUCKLER, H. KRIEG, H. LUKAS, G. PETZOW and J. WEISS, *Calphad* **3** (1979) 241.

Received 18 July 1994
and accepted 22 March 1995